THE JOURNAL OF
PHYSICAL CHEMISTRY C

pubs.acs.org/JPCC Article

Influence of Dye Sensitizers on Charge Dynamics in SnO_2 Nanoparticles Probed with THz Spectroscopy

Jens Neu,* Sarah Ostresh, Kevin P. Regan, Jacob A. Spies, and Charles A. Schmuttenmaer*

Cite This: *J. Phys. Chem. C* 2020, 124, 3482−3488 Read Online

ACCESS | Metrics & More | Article Recommendations | Supporting Information

ABSTRACT: Using dye-sensitized water-splitting photoelectrochemical cells is a promising way to satisfy an increasing demand for energy without significant production of greenhouse gases. These cells commonly utilize a large band gap nanoparticulate semiconductor photoelectrode that is sensitized with a photoactive dye. In this paper, we study SnO_2 nanoparticles (NPs) that are sensitized with either a ruthenium-based dye (**RuP**) or a porphyrin-based dye (**Por**). These dyes have a significantly different molar extinction coefficient, resulting in either a high carrier density (**Por**) or a moderately low density (**RuP**) within the SnO_2 NPs. The influence of the dye on charge carrier dynamics and photoconductivity in the NPs has been explored. We present experimental results on samples of five different SnO_2 film thicknesses, sensitized with either **RuP** or **Por**. We find that the injection dynamics are very similar for both dyes, but the trapping dynamics strongly depend on the dye. We conclude that this dependence is linked to dye-induced surface states, electrostatic environment, and defects which increase carrier-trapping at the surface. Frequency-dependent measurements confirm that the dye influences the carrier dynamics in the NPs. This can be seen by the significant change in the Drude−Smith parameter *c*, which describes backscattering/localization effects at the surface. This parameter is approximately −0.9 for **RuP** and −0.8 for **Por**, showing a dependence on the chemical environment and the dye cation after injection.

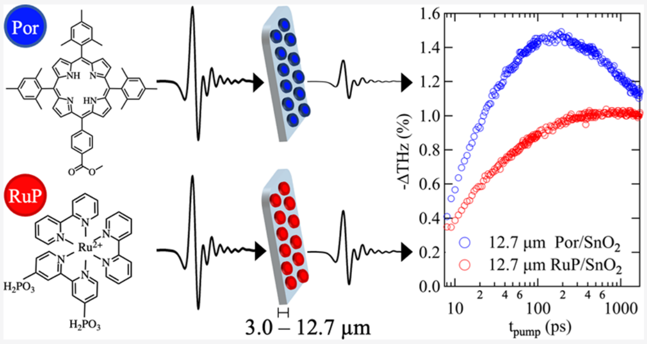

■ INTRODUCTION

Increasing concerns regarding climate change call for a significant reduction in CO_2 emission.[1] Wind and solar energies have the potential to satisfy the world's energy demands without greenhouse gas emission. However, a major challenge lies in developing methods to store this energy in sufficient amounts to meet energy needs in a nonintermittent manner.

One way to store large amounts of energy is to directly produce chemical fuels, such as hydrogen (H_2), which has a large energy density per unit mass,[2,3] or methanol, which is a liquid and easily transportable. Dye-sensitized nanoparticles (NPs) employed in photoelectrochemical cells are a promising avenue for direct conversion from photons to H_2.[4−9]

Wide band gap metal oxide semiconductor NPs act as a conductive host material, whereas visible light is harvested via photoexcitation of dye sensitizers, which subsequently inject electrons into the conduction band of the metal oxide. In a functional water-splitting dye-sensitized photoelectrochemical cell, hole transfer from the oxidized dye to water oxidation catalysts coadsorbed on the metal oxide occurs, consequently regenerating the dye. After four oxidizing equivalents are obtained, the water oxidation half-reaction occurs, releasing oxygen, protons, and electrons. Protons are subsequently reduced with the electrons at a dark cathode to form the desired product, H_2.

Optical pump terahertz probe (OPTP) experiments are an excellent way to study the generation and loss of conduction band electrons.[10,11] The change in terahertz (THz) signal with pump−probe delay (ΔTHz) reveals injection and trapping dynamics in the metal oxide. This is a crucial parameter that is sometimes correlated to the performance of solar devices.[12,13] In general, the goal is to maximize injection rates while minimizing trapping and recombination rates.

Additionally, frequency-dependent measurements provide a detailed picture of material parameters. In combination with conductivity models, such as Drude−Smith (DS),[14] it is possible to determine the carrier density, scattering time, and degree of backscattering/localization. We would like to emphasize that localization refers to a mobile electron that has a reduced probability of traveling/tunneling to another NP, and does not refer to trapping.

Received: November 25, 2019
Revised: January 12, 2020
Published: January 13, 2020

https://dx.doi.org/10.1021/acs.jpcc.9b11024
J. Phys. Chem. C 2020, 124, 3482−3488

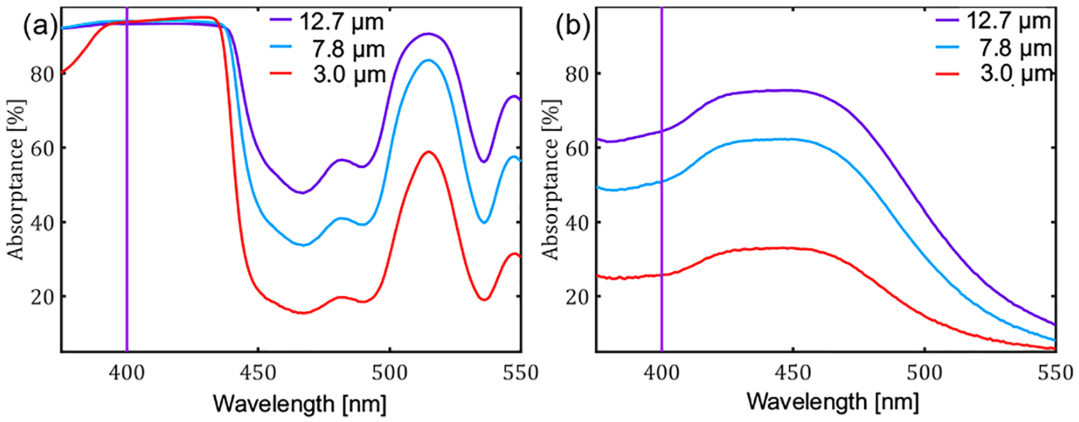

Figure 1. UV−vis measurements of sensitized film samples collected in integrating sphere configuration. In the **Por** case (a), the absorption length at 400 nm is about 1 μm, whereas for **RuP** (b), it is about 15 μm. Reprinted from[17] with the permission of AIP Publishing.

The scattering time defines the carrier mobility, and, in combination with the trapping lifetime, determines the diffusion length of free carriers in the metal oxide. The backscattering/localization parameter is a measure of the deviation from ideal Drude-like behavior and suppression of the dc conductivity. This parameter is sensitive to tunneling and other surface processes, which strongly depend on surface chemistry and charges.

In this paper, we investigate the influence of two common dye sensitizers attached to the same SnO_2 NPs. We fabricated two sets of samples with thicknesses ranging from 3.0 to 12.7 μm, sensitized with either 5-4(methoxycarbonylphenyl)-10,15,20-tris(2,4,6-trimethyphenyl)-porphyrin (referred to as **Por**) or (4,4′-diphosphonato-2,2′-bipyridine)bis(2,2′-bipyridine)ruthenium(II)bromide (which is referred to as **RuP**). The dye structures are provided in the Supporting Information. **Por** is a very strongly absorbing dye, whereas **RuP** is only moderately absorbing (roughly 10 times less than **Por**). This leads to a large difference in the penetration depth of the pump beam into the SnO_2 NP film (sometimes referred to as the optical skin depth).

Specifically, the penetration depth for weak excitation at a 400 nm wavelength is approximately 1 μm for **Por**, and 15 μm for **RuP**. This difference has a significant influence on carrier concentration, which allows us to access different photodoping regimes without adjusting the laser fluence.

■ EXPERIMENTAL SECTION

Sample Preparation. Mesoporous SnO_2 films were prepared using a standard doctor-blading procedure of a metal oxide paste. The SnO_2 paste was prepared as previously described[15] using commercially available SnO_2 NPs (Sigma-Aldrich) ranging in diameter from 22 to 43 nm. This paste was doctor-bladed onto fused quartz slides as previously described[16] using Scotch tape as the spacer followed by annealing for 10 min at 80 °C. Thicker films were prepared by alternating additional doctor-blading steps and annealing. After the desired film thickness was achieved, SnO_2 films were annealed at 370 °C for 10 min, followed by a second annealing step at 470 °C for 30 min. Temperatures were ramped by 3 °C per minute. The resulting films had thicknesses of 3.0 ± 0.5, 5.7 ± 0.6, 7.8 ± 1.3, 10.7 ± 0.3, and 12.7 ± 1 μm as determined by mechanical profilometry for the one-, two-, three-, four-, and five-layer samples, respectively.

Por/SnO_2 samples were sensitized in the dark in a 0.18 mM solution of **Por** in dicholoromethane for 9 h at room temperature.[18] **RuP**/SnO_2 samples were sensitized in the dark in a 0.1 mM solution of **RuP** in dry ethanol for 22 h at room temperature.[19,20] Figure 1 displays UV−vis spectra of three representative film thicknesses, which allows the absorption skin depths at 400 nm to be determined (less than 1 μm for **Por** and approximately 15 μm for **RuP**).

Spectroscopic Measurements. The samples were measured in an OPTP spectrometer as previously described.[17] This spectrometer utilizes the output of a titanium:sapphire-amplifier with a center wavelength of 800 nm, 1 kHz repetition rate, 35 fs average pulse width, and 4 mJ pulse energy. The output pulse was split into three beams for THz generation, THz detection, and optical photoexcitation, respectively. THz radiation was generated in a two-color air plasma[21] and subsequently detected using electro-optical sampling in ZnTe.[22,23] The optical photoexcitation beam was frequency doubled in a β-barium borate crystal. The resulting output at 400 nm has a Gaussian spatial distribution, a pulse energy of 150 μJ, and a full width at half-maximum (fwhm) of 8.6 mm. This diameter is significantly larger than the THz spot size, which is collimated to approximately 1.5 mm in diameter. Thus, the pump fluence in the THz probe region is 1.96 mJ/cm^2.

Two different types of measurement are presented in this paper. The first type detects the THz-peak amplitude change for different pump delays (denoted by OPTP).[10,24,25] These measurements provide insight into charge injection and trapping dynamics. The second type measures the complete THz-transient at a given pump−probe delay time. These measurements are Fourier transformed to yield the frequency-dependent THz photoconductivity spectrum and are referred to as time-resolved THz spectroscopy (TRTS).[10,26,27]

■ RESULTS AND DISCUSSION

Optical Pump Terahertz Probe. We measured the OPTP traces of both **RuP** and **Por** sample sets. The THz change versus pump delay time measured in the **RuP** samples is plotted in Figure 2. As the sample thickness increases, the THz signal increases as well. This can be understood when we consider that the optical penetration depth of **RuP** is $\delta \approx$ 15 μm. All of the samples are thinner than this, and as a result only a fraction of the optical excitation is absorbed by the sample, as described by Beer's law

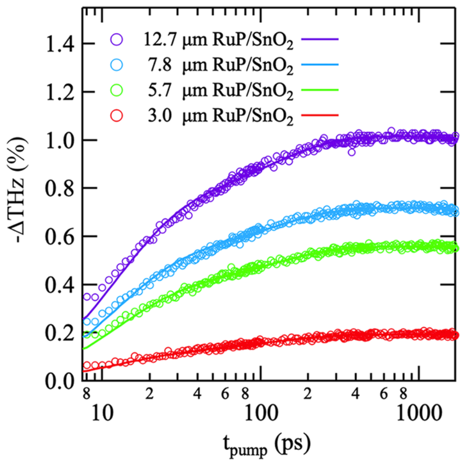

Figure 2. OPTP traces of **RuP**-sensitized SnO_2. Although the total signal increases for thicker samples, injection dynamics are independent of the layer thickness. The solid lines show a fit of the model to the data using eq 2. The global fit uses the same injection time constant for all samples, independent of layer thickness.

$$A = I_{abs}/I_0 = 1 - e^{-d/\delta} \tag{1}$$

with d being the sample thickness, δ being the optical penetration depth, A being the absorptance, not to be confused with the absorbance, and I_{abs}/I_0 the fraction of the total incident power I_0 absorbed.

For the thinnest layer, only 26% of the incident photons are absorbed, whereas for the thickest sample, 64% are absorbed (see Figure 1). As a result, the total number of excited dye molecules increases with increasing layer thickness, and therefore the total number of carriers injected into the samples increases as well. A larger number of carriers in thicker films results in reduced transmittance as observed in Figure 2.

The dynamics of injection and trapping are described by

$$\Delta\mathrm{THz}(t) = (A_1[e^{(t/\tau_1)} - 1] + A_2[e^{(t/\tau_2)} - 1] - A_3[e^{(t/\tau_3)} - 1]) \otimes G_R \tag{2}$$

where A_1 and A_2 are the injection amplitudes and A_3 is the trapping amplitude. The injection and recombination/trapping times are given by τ_1, τ_2, and τ_3. The global fit considers all OPTP traces for a given dye on the films of varying thickness, and enforces that the injection times are identical. The sum of injection ($A_1 + A_2$) must be equal to the sum of the recombination/trapping (A_3). Furthermore, the equation is convoluted with the instrument response function (G_R), which describes a Gaussian instrument response with fwhm of 0.6 ps.[28]

The trapping lifetime depends on the total layer thickness, as seen in Table 1. To understand this, we consider several possible trapping mechanisms. First, the electron can interact with another electron and undergo a trap-assisted Auger process,[29−31] which will be nonlinear with carrier concentration. Second, the electron can be captured by traps. This effect depends on the abundance of unoccupied trap states relative to the carrier density. The trap state density is a material parameter and in the case of NPs, it is primarily dominated by the electrostatic environment, surface states, and the chemical environment around these states.[32] Recombination is also possible as a third mechanism. However, transient absorption measurements on similar systems showed that recombination typically occurs on a microsecond timescale, which is significantly slower than the dynamics reported here.[33−36]

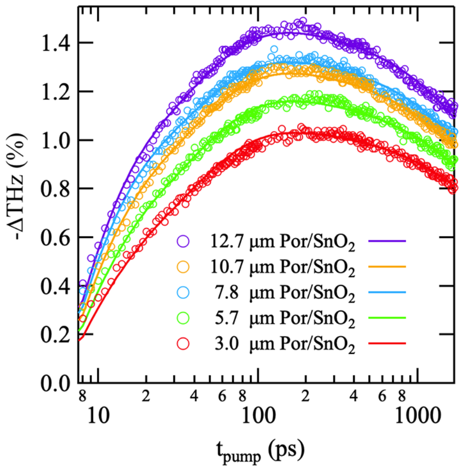

Figure 3. OPTP traces of **Por**-sensitized SnO_2. Although the total signal increases for thicker samples, injection dynamics are independent of the layer thickness. The solid lines show a global fit of the model to the data using eq 2 and also globally fitting all of the samples simultaneously wherein there are identical injection dynamics independent of layer thickness.

In the thinner layers, the carrier density is larger. Therefore, Auger and trap-assisted Auger recombination would result in a shorter lifetime, but experimental results show the opposite trend. Furthermore, the carrier density is rather moderate, as shown later for the TRTS results, in Figure 5a. Therefore, we conclude that Auger is not a dominant recombination process in these samples.

The trap density for all of the layer thicknesses is identical, given that the material is the same and all processing steps are identical. As a result, the ratio between trap density and carrier density will scale directly with carrier density. If the carrier density is noticeably larger than the trap density, the traps will saturate and the influence of this channel will decrease. The charges will therefore live longer, which explains the larger lifetime for the thinner samples, summarized in Table 1.

The OPTP traces of **Por**-sensitized samples are plotted in Figure 3. The first notable result is that despite the short optical penetration depth of approximately 1 μm, the sample thickness has a non-negligible influence on the overall signal. The absorption coefficient was determined with low power continuous wave exposure (i.e., a UV−vis spectrometer). This technique differs from the conditions of OPTP in which an ultrashort high-flux laser pulse is used, which results in saturation of the dye sensitizers. This increases the transmission of the sample compared to the low power values.

Similar to **RuP**, the increase in layer thickness results in an increase in the number of carriers, which results in a reduced THz transmission, visible in Figure 3. In comparison to **RuP**-sensitized films, in which the transmission changed by a factor of 5, the change in **Por** is only 1.3 times. This shows that the majority of photon absorption and charge injection takes place in the first few micrometers of the sample, and hence simply adding more material does not result in a significant increase in conductivity.

As the majority of charges are generated in the first few micrometers of the sample, the trapping lifetime dependence on the layer thickness is less pronounced (Table 1). We notice

Table 1. Carrier-Trapping Lifetime (τ_3) from Best Fit Described by eq 2[a]

sample/thickness	3.0 ± 0.5 μm	5.7 ± 0.6 μm	7.8 ± 1.3 μm	7.8 ± 1.3 μm	12.7 ± 1.1 μm
τ_3 (**RuP**) in ns	≫100	≫100	130 ± 14		133 ± 11
τ_3 (**Por**) in ns	6.20 ± 0.04	6.20 ± 0.04	5.50 ± 0.02	5.41 ± 0.02	5.36 ± 0.02

[a] For the **RuP** samples, a correlation between layer thickness and lifetime is evident, which is explained as trap-state depletion. For the **Por** samples, the same trend is observed, but is less pronounced.

a small reduction of the carrier lifetime with increasing sample thickness, which is linked to the aforementioned trap-state depletion.

The thickest layers' results are used to compare the two different sensitizers, as these exhibit the best signal to noise ratio and hence the smallest uncertainty. The trapping lifetime in SnO_2 sensitized with **RuP** is more than 16 times longer than in the **Por** case. This is a potential indicator that different sensitizers not only change the carrier injection, but also the trap density in the material itself, in particular the surface states and the dielectric environment of the NP. The influence that the sensitizer has on the NPs can be understood in more detail when evaluating the frequency-dependent photoconductivity data.

Time-Resolved Terahertz Spectroscopy. A more comprehensive description of photoconductivity in dye-sensitized NPs can be gained by measuring their frequency-dependent conductivity. TRTS scans were performed 900, 1300, and 1800 ps after photoexcitation. The trends for each of these delay times are similar (see Supporting Information), hence this discussion focuses solely on the 1300 ps results.

The TRTS data provide the frequency-dependent change in THz transmission upon photoexcitation. The corresponding conductivity change from these experiments is obtained using the data-processing procedure as described in detail in previous publications[17,37] (and an overview is provided in the Supporting Information), rather than the thin-film equation,[38] which is not reliable for these samples.[17]

In short, the time-resolved photoconductivity is obtained by comparing the transmission through a sample after photo-excitation to that without photoexcitation. However, the thickness of the photoexcited layer has a large influence on the parameters extracted.[17] One of the issues in analyzing the data is that the two types of samples studied here have different optical absorption lengths. For the weakly absorbing **RuP** dye, essentially the entire thickness is photoexcited, whereas, for the highly absorbing **Por** dye, the photoexcitation occurs at the front surface, leaving behind a layer of non-photoexcited material.

The photoconductivity for representative **Por** and **RuP** samples are plotted in Figure 4. The photoconductivity spectrum exhibits a positive real part in conductivity as well as a negative imaginary part, a behavior well-known from TRTS measurements of photoexcited nanogranular semi-conductors beginning 17 years ago.[26]

To obtain information regarding carrier density and carrier mobility, the DS model[14,26,39,40] was chosen. It is a variation of the classic Drude model of conductivity that has an additional term. It was proposed by Smith in 2001.[14] The first part of eq 3 is the standard Drude model, and the second part (in parentheses with the additional c parameter) accounts for localization/backscattering because of grain boundaries in NP films. It has provided reliable results in many previous experiments with similar materials.[6,37,41,42] The complex-valued conductivity is given by

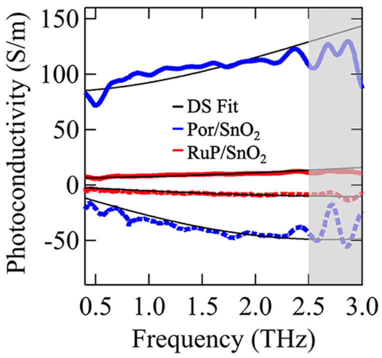

Figure 4. Photoconductivity for 12.6 μm thick samples at a delay time of 1300 ps with either **Por** (blue) or **RuP** (red) sensitizer. The solid lines show the best fit results using the DS eq 3.

$$\sigma = \frac{Ne^2\tau_s/m^*}{1 - i\omega\tau_s}\left(1 + \frac{c}{1 - i\omega\tau_s}\right) \tag{3}$$

The DS model provides information on the carrier density N, the carrier scattering time (τ_s), and the DS parameter c, which is related to carrier localization/backscattering. We would like to emphasize that this parameter is not linked to the lifetime; electrons that scatter with the interface do not necessarily recombine or become trapped. An effective mass of $m^* = 0.275m_e$ was used, where m_e is the electron mass.[43,44]

The scattering time, τ_s, extracted from the DS model is plotted in Figure 5b. This value describes the mean time between two elastic scattering processes for an electron. This time ranges from 16 to 23 fs for **RuP** to 18 and 25 fs for **Por**.

The carrier scattering time for all samples is nearly identical within experimental uncertainty. There are several mechanisms that result in carrier scattering, including impurities, grain boundaries, phonons, and electrons. The fact that the scattering time is not correlated to the carrier density demonstrates that electron−electron scattering plays only a minor role at the pump fluences used in this work. This result justifies neglecting the influence of Auger processes as previously discussed for the OPTP results.

The different sensitizers do not have a significant influence on the scattering rate. This indicates that the electrostatic environment, which is influenced by the dyes bound to the surface, does not play an important role in bulk-like scattering processes described by τ_s.

The final parameter of the DS model is the c parameter. Although there has been significant debate over the last 15 years regarding the precise meaning of this parameter, recent work employing rigorous Monte Carlo simulations,[39] as well as the original derivation of this parameter,[14] attribute it to charge scattering occurring at grain boundaries, and the dielectric environment. The experimental results for the c parameter are plotted in Figure 5c. While there is a small variation in the c parameter for the five **Por** samples and the

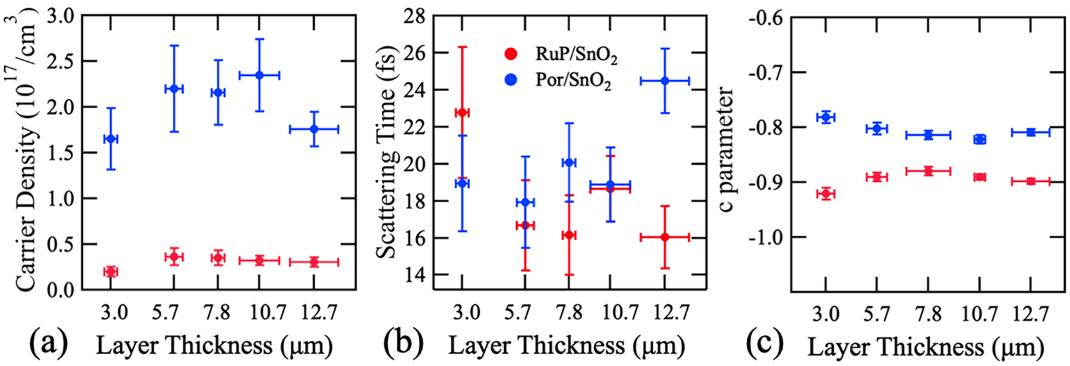

Figure 5. Carrier density N, scattering time τ_s, and c-parameter from best-fit results using the DS eq 3. (a) Carrier density strongly depends on the penetration depth and sample thickness, resulting in a significantly higher density for **Por** compared to **RuP**. (b) Scattering time is within the uncertainty independent of layer thickness and sensitizer, confirming that this parameter describes the bulk properties of SnO$_2$. (c) The c parameter describes the backscattering/localization and depends on the dielectric environment of the NPs.[45] This illustrates the influence of the two sensitizers on the NPs.

five **RuP** samples, the c parameter does not show a clear dependence on layer thickness and carrier density.

Comparison of the two different sensitizers shows a small difference between the c parameters, which are either $c = -0.78$ to -0.82 in **Por** or $c = -0.88$ to -0.92 in **RuP**. This difference might seem counterintuitive at first, as the c parameter should be a material parameter and identical SnO$_2$ NPs were used as the starting material in the sample preparation. However, this parameter is not a mere geometrical parameter but is also linked to the electrostatic potentials at the interface.[45] Electrostatic charges will alter the potential barrier for grain-to-grain tunneling.[32,45,46]

The tunneling barrier can depend on the chemical surrounding of the NP necking regions, including charges and polarization effects of the ionized dye.[45] This depends on the chemical composition of the dye and its linkers, which determines the distance between the charged region of the dye and the surface, and the dye deposition conditions (i.e., solvent and temperature). Whereas the majority of research studies on dye sensitizers are focused on increasing injection yield and sample coverage, the influence the dye itself has on the material is frequently ignored. This result demonstrates that the influence of the dye on the electronic structure of the metal oxide is not negligible and must be considered, in particular, as the c parameter is crucial for the dc conductivity of the film.

■ CONCLUSIONS

Dye-sensitized NPs have received significant attention in recent years. However, the few studies that compare different dyes focus solely on the dynamics of injection and recombination. In this paper, two commonly used dyes are compared with a particular focus on the influence that these dyes have on the material parameters of the host material. The dyes used were **Por**, with a penetration length of $\delta \approx 1$ μm, and **RuP**, with $\delta \approx 15$ μm.

We have presented OPTP traces of SnO$_2$ NPs sensitized with two different dyes with thicknesses ranging from 3.0 to 12.7 μm. We find that for moderately absorbing dyes such as **RuP**, which leads to a large penetration depth, the thicker films resulted in an increase in THz signal because of an increase in total absorption. The same trend, albeit less pronounced, is found for the **Por** dye. Based on the OPTP results, we conclude that the dominant trapping mechanism is linked to trap states and trap state depletion, not Auger processes.

In addition to OPTP measurements, frequency-dependent TRTS measurements were performed. We employed the DS model to extract the carrier density (N), scattering time (τ_s), and the backscattering/localization parameter (c). We find that the bulk scattering time is largely independent of the dye, but the c parameter depends on it. This dependence is explained by the influence that the dye has on the electrostatics near the surface in SnO$_2$. As the c parameter is very important for dc performance, it is crucial to consider it when comparing different dyes and not simply assume that it depends only on the host material (SnO$_2$).

For the design of effective photoelectrochemical cells, it is important to not only match the energy levels and density of states for charge injection, but also to consider the influence of the dye on trap and surface states. The chemical linkers and the polarizability of the dye influence local permittivity, which in turn changes the particle to particle conductivity. Furthermore, surface passivation layers provide a promising approach to achieve efficient light-harvesting and long-living mobile carriers. Choosing the best materials for photo-elctrochemistry therefore involves considering all these effects.

■ ASSOCIATED CONTENT

Supporting Information

The Supporting Information is available free of charge at https://pubs.acs.org/doi/10.1021/acs.jpcc.9b11024.

> Chemical structures of **RuP** and **Por**; potential estimated at neutral pH relative to NHE; conductivity traces and conductivity parameters for different time delays; the 649 nm absorbance of **Por** dissolved at varying concentrations in toluene; normalized OPTP traces for **RuP**-sensitized and **Por**-sensitized SnO$_2$; fit parameters that describe the dynamics of trapping and injection; dye loadings of each sample; the calculated rations between photons and molecules; and carrier density, scattering time, and c parameter of each sample at three time delays after injection (PDF)

■ AUTHOR INFORMATION

Corresponding Authors

Jens Neu − *Department of Chemistry and Microbial Science Institute (MSI), Yale University, New Haven 06520-8107,* *Connecticut, United States;* orcid.org/0000-0002-1054-0444; Email: jens.neu@yale.edu

Charles A. Schmuttenmaer – *Department of Chemistry and Energy Science Institute (ESI), Yale University, New Haven 06520-8107, Connecticut, United States;* orcid.org/0000-0001-9992-8578; Email: charles.schmuttenmaer@yale.edu

Authors

Sarah Ostresh – *Department of Chemistry and Energy Science Institute (ESI), Yale University, New Haven 06520-8107, Connecticut, United States*

Kevin P. Regan – *Department of Chemistry and Energy Science Institute (ESI), Yale University, New Haven 06520-8107, Connecticut, United States;* orcid.org/0000-0003-3522-092X

Jacob A. Spies – *Department of Chemistry and Energy Science Institute (ESI), Yale University, New Haven 06520-8107, Connecticut, United States;* orcid.org/0000-0002-0148-4823

Complete contact information is available at:
https://pubs.acs.org/10.1021/acs.jpcc.9b11024

Notes

The authors declare no competing financial interest.

■ ACKNOWLEDGMENTS

We acknowledge financial support from the NSF: National Science Foundation under grant number NSF CHE—CSDMA 1465085, and the U.S. Department of Energy Office of Science, Office of Basic Energy Sciences, under award DE-FG02-07ER15909, as well as from a generous donation from the TomKat Foundation. J.A.S. acknowledges support from the Onsager Graduate Research Fellowship in Chemistry. We would like to thank Dr. Shin-Hee Lee for supplying the dyes used.

■ REFERENCES

(1) Shakun, J. D.; Clark, P. U.; He, F.; Marcott, S. A.; Mix, A. C.; Liu, Z.; Otto-Bliesner, B.; Schmittner, A.; Bard, E. Global warming preceded by increasing carbon dioxide concentrations during the last deglaciation. *Nature* **2012**, *484*, 49.

(2) Turner, J. A. A Realizable Renewable Energy Future. *Science* **1999**, *285*, 687–689.

(3) Tachibana, Y.; Vayssieres, L.; Durrant, J. R. Artificial photosynthesis for solar water-splitting. *Nat. Photonics* **2012**, *6*, 511.

(4) Grätzel, M. Dye-sensitized solar cells. *J. Photochem. Photobiol., C* **2003**, *4*, 145–153.

(5) Mathew, S.; Yella, A.; Gao, P.; Humphry-Baker, R.; Curchod, B. F. E.; Ashari-Astani, N.; Tavernelli, I.; Rothlisberger, U.; Nazeeruddin, M. K.; Grätzel, M. Dye-sensitized solar cells with 13% efficiency achieved through the molecular engineering of porphyrin sensitizers. *Nat. Chem.* **2014**, *6*, 242.

(6) Regan, K. P.; Swierk, J. R.; Neu, J.; Schmuttenmaer, C. A. Frequency-Dependent Terahertz Transient Photoconductivity of Mesoporous SnO_2 Films. *J. Phys. Chem. C* **2017**, *121*, 15949–15956.

(7) Spies, J. A.; Perets, E. A.; Fisher, K. J.; Rudshteyn, B.; Batista, V. S.; Brudvig, G. W.; Schmuttenmaer, C. A. Collaboration between experiment and theory in solar fuels research. *Chem. Soc. Rev.* **2019**, *48*, 1865–1873.

(8) Brennaman, M. K.; Dillon, R. J.; Alibabaei, L.; Gish, M. K.; Dares, C. J.; Ashford, D. L.; House, R. L.; Meyer, G. J.; Papanikolas, J. M.; Meyer, T. J. Finding the Way to Solar Fuels with Dye-Sensitized Photoelectrosynthesis Cells. *J. Am. Chem. Soc.* **2016**, *138*, 13085–13102.

(9) Swierk, J. R.; Mallouk, T. E. Design and development of photoanodes for water-splitting dye-sensitized photoelectrochemical cells. *Chem. Soc. Rev.* **2013**, *42*, 2357–2387.

(10) Beard, M. C.; Turner, G. M.; Schmuttenmaer, C. A. Transient photoconductivity in GaAs as measured by time-resolved terahertz spectroscopy. *Phys. Rev. B: Condens. Matter Mater. Phys.* **2000**, *62*, 15764–15777.

(11) Beard, M. C.; Turner, G. M.; Schmuttenmaer, C. A. Subpicosecond carrier dynamics in low-temperature grown GaAs as measured by time-resolved terahertz spectroscopy. *J. Appl. Phys.* **2001**, *90*, 5915–5923.

(12) Tiwana, P.; Docampo, P.; Johnston, M. B.; Snaith, H. J.; Herz, L. M. Electron Mobility and Injection Dynamics in Mesoporous ZnO, SnO_2, and TiO_2 Films Used in Dye-Sensitized Solar Cells. *ACS Nano* **2011**, *5*, 5158–5166.

(13) Li, G.; Richter, C. P.; Milot, R. L.; Cai, L.; Schmuttenmaer, C. A.; Crabtree, R. H.; Brudvig, G. W.; Batista, V. S. Synergistic effect between anatase and rutile TiO2 nanoparticles in dye-sensitized solar cells. *Dalton Trans.* **2009**, 10078–10085.

(14) Smith, N. Classical generalization of the Drude formula for the optical conductivity. *Phys. Rev. B: Condens. Matter Mater. Phys.* **2001**, *64*, 155106.

(15) Ito, S.; Chen, P.; Comte, P.; Nazeeruddin, M. K.; Liska, P.; Péchy, P.; Grätzel, M. Fabrication of screen-printing pastes from TiO_2 powders for dye-sensitised solar cells. *Prog. Photovolt. Res. Appl.* **2007**, *15*, 603–612.

(16) Swierk, J. R.; McCool, N. S.; Nemes, C. T.; Mallouk, T. E.; Schmuttenmaer, C. A. Ultrafast Electron Injection Dynamics of Photoanodes for Water-Splitting Dye-Sensitized Photoelectrochemical Cells. *J. Phys. Chem. C* **2016**, *120*, 5940–5948.

(17) Neu, J.; Regan, K. P.; Swierk, J. R.; Schmuttenmaer, C. A. Applicability of the Thin-film Approximation in Terahertz Photoconductivity Measurements. *Appl. Phys. Lett.* **2018**, *113*, 233901.

(18) Lee, S. H.; Regan, K. P.; Hedström, S.; Matula, A. J.; Chaudhuri, S.; Crabtree, R. H.; Batista, V. S.; Schmuttenmaer, C. A.; Brudvig, G. W. Linker Length-Dependent Electron-Injection Dynamics of Trimesitylporphyrins on SnO_2 Films. *J. Phys. Chem. C* **2017**, *121*, 22690–22699.

(19) Swierk, J. R.; McCool, N. S.; Mallouk, T. E. Dynamics of Electron Recombination and Transport in Water-Splitting Dye-Sensitized Photoanodes. *J. Phys. Chem. C* **2015**, *119*, 13858–13867.

(20) Swierk, J. R.; Regan, K. P.; Jiang, J.; Brudvig, G. W.; Schmuttenmaer, C. A. Rutile TiO_2 as an Anode Material for Water-Splitting Dye-Sensitized Photoelectrochemical Cells. *ACS Energy Lett.* **2016**, *1*, 603–606.

(21) Kress, M.; Löffler, T.; Eden, S.; Thomson, M.; Roskos, H. G. Terahertz-pulse generation by photoionization of air with laser pulses composed of both fundamental and second-harmonic waves. *Opt. Lett.* **2004**, *29*, 1120–1122.

(22) van der Valk, N. C. J.; Wenckebach, T.; Planken, P. C. M. Full mathematical description of electro-optic detection in optically isotropic crystals. *J. Opt. Soc. Am. B* **2004**, *21*, 622–631.

(23) Wu, Q.; Zhang, X. C. Free-space electro-optic sampling of terahertz beams. *Appl. Phys. Lett.* **1995**, *67*, 3523–3525.

(24) Neu, J.; Rahm, M. Terahertz time domain spectroscopy for carrier lifetime mapping in the picosecond to microsecond regime. *Opt. Express* **2015**, *23*, 12900–12909.

(25) George, P. A.; Strait, J.; Dawlaty, J.; Shivaraman, S.; Chandrashekhar, M.; Rana, F.; Spencer, M. G. Ultrafast Optical-Pump Terahertz-Probe Spectroscopy of the Carrier Relaxation and Recombination Dynamics in Epitaxial Graphene. *Nano Lett.* **2008**, *8*, 4248–4251.

(26) Turner, G. M.; Beard, M. C.; Schmuttenmaer, C. A. Carrier Localization and Cooling in Dye-Sensitized Nanocrystalline Titanium Dioxide. *J. Phys. Chem. B* **2002**, *106*, 11716–11719.

(27) Iwaszczuk, K.; Cooke, D. G.; Fujiwara, M.; Hashimoto, H.; Uhd Jepsen, P. Simultaneous reference and differential waveform acquisition in time-resolved terahertz spectroscopy. *Opt. Express* **2009**, *17*, 21969–21976.

(28) Regan, K. P.; Koenigsmann, C.; Sheehan, S. W.; Konezny, S. J.; Schmuttenmaer, C. A. Size-Dependent Ultrafast Charge Carrier Dynamics of WO3 for Photoelectrochemical Cells. *J. Phys. Chem. C* **2016**, *120*, 14926−14933.

(29) Cohn, A. W.; Schimpf, A. M.; Gunthardt, C. E.; Gamelin, D. R. Size-Dependent Trap-Assisted Auger Recombination in Semiconductor Nanocrystals. *Nano Lett.* **2013**, *13*, 1810−1815.

(30) Landsberg, P. T.; Rhys-Roberts, C.; Lal, P. Auger recombination and impact ionization involving traps in semiconductors. *Proc. Phys. Soc.* **1964**, *84*, 915.

(31) Milot, R. L.; Sutton, R. J.; Eperon, G. E.; Haghighirad, A. A.; Martinez Hardigree, J.; Miranda, L.; Snaith, H. J.; Johnston, M. B.; Herz, L. M. Charge-Carrier Dynamics in 2D Hybrid Metal-Halide Perovskites. *Nano Lett.* **2016**, *16*, 7001−7007.

(32) Ibach, H. *Physics of Surfaces and Interfaces*; Springer, 2006.

(33) Green, A. N. M.; Palomares, E.; Haque, S. A.; Kroon, J. M.; Durrant, J. R. Charge Transport versus Recombination in Dye-Sensitized Solar Cells Employing Nanocrystalline TiO_2 and SnO_2 Films. *J. Phys. Chem. B* **2005**, *109*, 12525−12533.

(34) Gish, M. K.; Lapides, A. M.; Brennaman, M. K.; Templeton, J. L.; Meyer, T. J.; Papanikolas, J. M. Ultrafast Recombination Dynamics in Dye-Sensitized SnO_2/TiO_2 Core/Shell Films. *J. Phys. Chem. Lett.* **2016**, *7*, 5297−5301.

(35) Jiang, J.; Spies, J. A.; Swierk, J. R.; Matula, A. J.; Regan, K. P.; Romano, N.; Brennan, B. J.; Crabtree, R. H.; Batista, V. S.; Schmuttenmaer, C. A.; et al. Direct Interfacial Electron Transfer from High-Potential Porphyrins into Semiconductor Surfaces: A Comparison of Linkers and Anchoring Groups. *J. Phys. Chem. C* **2018**, *122*, 13529−13539.

(36) Jiang, J.; Swierk, J. R.; Materna, K. L.; Hedström, S.; Lee, S. H.; Crabtree, R. H.; Schmuttenmaer, C. A.; Batista, V. S.; Brudvig, G. W. High-Potential Porphyrins Supported on SnO_2 and TiO_2 Surfaces for Photoelectrochemical Applications. *J. Phys. Chem. C* **2016**, *120*, 28971−28982.

(37) Neu, J.; Schmuttenmaer, C. A. Tutorial: An Introduction to Terahertz Time Domain Spectroscopy (THz-TDS). *J. Appl. Phys.* **2018**, *124*, 231101.

(38) Glover, R. E.; Tinkham, M. Conductivity of Superconducting Films for Photon Energies between 0.3 and $40kT_c$. *Phys. Rev.* **1957**, *108*, 243−256.

(39) Cocker, T. L.; Baillie, D.; Buruma, M.; Titova, L. V.; Sydora, R. D.; Marsiglio, F.; Hegmann, F. A. Microscopic origin of the Drude-Smith model. *Phys. Rev. B* **2017**, *96*, 205439.

(40) Baxter, J. B.; Schmuttenmaer, C. A. Conductivity of ZnO Nanowires, Nanoparticles, and Thin Films Using Time-Resolved Terahertz Spectroscopy. *J. Phys. Chem. B* **2006**, *110*, 25229−25239.

(41) Cooke, D. G.; MacDonald, A. N.; Hryciw, A.; Wang, J.; Li, Q.; Meldrum, A.; Hegmann, F. A. Transient terahertz conductivity in photoexcited silicon nanocrystal films. *Phys. Rev. B: Condens. Matter Mater. Phys.* **2006**, *73*, 193311.

(42) Ulbricht, R.; Hendry, E.; Shan, J.; Heinz, T. F.; Bonn, M. Carrier dynamics in semiconductors studied with time-resolved terahertz spectroscopy. *Rev. Mod. Phys.* **2011**, *83*, 543−586.

(43) Schleife, A.; Varley, J. B.; Fuchs, F.; Rödl, C.; Bechstedt, F.; Rinke, P.; Janotti, A.; Van de Walle, C. G. Tin dioxide from first principles: Quasiparticle electronic states and optical properties. *Phys. Rev. B: Condens. Matter Mater. Phys.* **2011**, *83*, 035116.

(44) Button, K. J.; Fonstad, C. G.; Dreybrodt, W. Determination of the Electron Masses in Stannic Oxide by Submillimeter Cyclotron Resonance. *Phys. Rev. B: Condens. Matter Mater. Phys.* **1971**, *4*, 4539−4542.

(45) Konezny, S. J.; Richter, C.; Snoeberger, R. C.; Parent, A. R.; Brudvig, G. W.; Schmuttenmaer, C. A.; Batista, V. S. Fluctuation-Induced Tunneling Conductivity in Nanoporous TiO2 Thin Films. *J. Phys. Chem. Lett.* **2011**, *2*, 1931−1936.

(46) Batzill, M.; Diebold, U. The surface and materials science of tin oxide. *Prog. Surf. Sci.* **2005**, *79*, 47−154.